Negative Differential Photoconductance in Gold Nanoparticle Arrays in the Coulomb Blockade Regime

Markus A. Mangold,[†,‡] Michel Calame,[§] Marcel Mayor,[⊥] and Alexander W. Holleitner[†,*]

[†]Walter Schottky Institut and Physik-Department, Technische Universität München, Am Coulombwall 4a, 85748 Garching, Germany, [‡]Laboratory for Air Pollution and Environmental Technology, Swiss Federal Laboratories for Materials Testing and Research, Empa, Uberlandstr. 129, 8600 Dübendorf, Switzerland, [§]Departement Physik, Universität Basel, Klingelbergstrasse 82, 4056 Basel, Switzerland, and [⊥]Departement Chemie, Universität Basel, St. Johanns-Ring 19, 4056 Basel, Switzerland

ABSTRACT

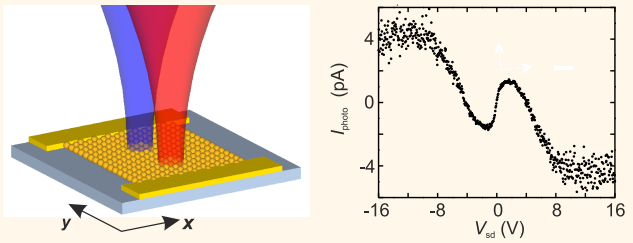

We investigate the photoconductance of gold nanoparticle arrays in the Coulomb blockade regime. Two-dimensional, hexagonal crystals of nanoparticles are produced by self-assembly. The nanoparticles are weakly coupled to their neighbors by a tunneling conductance. At low temperatures, the single electron charging energy of the nanoparticles dominates the conductance properties of the array. The Coulomb blockade of the nanoparticles can be lifted by optical excitation with a laser beam. The optical excitation leads to a localized heating of the arrays, which in turn gives rise to a local change in conductance and a redistribution of the overall electrical potential in the arrays. We introduce a dual-beam optical excitation technique to probe the distribution of the electrical potential in the nanoparticle array. A negative differential photoconductance is the direct consequence of the redistribution of the electrical potential upon lifting of the Coulomb blockade. On the basis of our model, we calculate the optically induced current from the dark current–voltage characteristics of the nanoparticle array. The calculations closely reproduce the experimental observations.

KEYWORDS: nanoparticles · nanoparticle assemblies · Coulomb blockade · photoconductance · nanoscale optoelectronics · photothermoelectrics

Arrays of metal nanoparticles in an organic matrix have attracted a lot of interest due to their diverse electronic properties.[1,2] By varying parameters such as the nanoparticle material, the matrix material, the nanoparticle size, and the interparticle distance, the electronic behavior of the nanoparticle array can be substantially tuned and controlled. For strong tunnel coupling between adjacent nanoparticles, the assembly exhibits conductance properties similar to the bulk properties of the nanoparticle material. For instance, assemblies from conducting nanoparticles show an Ohmic transport behavior,[3] while superconductivity is observed in assemblies from strongly coupled superconducting nanoparticles.[4] When the coupling between the nanoparticles is reduced, a metal–insulator transition is observed in the overall assembly.[5−7] In insulating nanoparticle arrays where the individual particles are only weakly coupled to neighboring particles, the single electron charging energy E_c of a nanoparticle can govern the electron transport.[8−10] The transport through the array is blocked, unless an energy of E_c is provided to the electrons by thermal activation or an applied bias. This is the so-called Coulomb blockade. Arrays in the Coulomb blockade regime are interesting for electronic applications due to their highly nonlinear current–voltage characteristics.[11,12]

Here, we report on the investigation of the photoconductance of gold nanoparticle arrays in the Coulomb blockade regime. At room temperature, the photoconductance of gold nanoparticle arrays can be dominated by bolometric conductance enhancement,[13] plasmonic field enhancement,[14] and trap state filling in the nanoparticle cores.[15] We show that in the Coulomb blockade regime, the photoconductance is governed by a redistribution of the potential landscape in the nanoparticle array. We optically excite the nanoparticle array with a focused laser beam. Due to absorption of the incident light, we locally heat up the nanoparticle array. The inhomogeneous temperature profile leads to a redistribution of

* Address correspondence to holleitner@wsi.tum.de.

Received for review February 14, 2012 and accepted April 12, 2012.

Published online April 12, 2012
10.1021/nn300673t

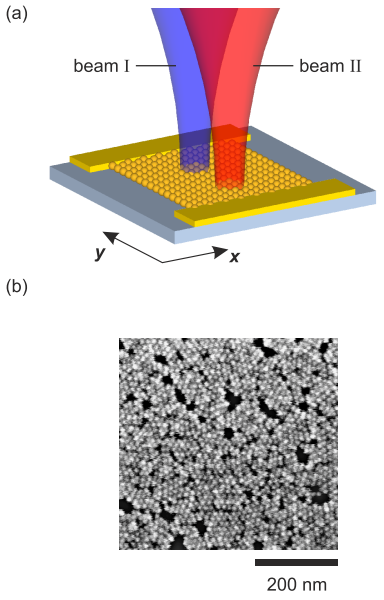

Figure 1. (a) Sketch of an electrically contacted gold nanoparticle array irradiated by two laser beams. (b) Scanning electron microscope (SEM) image of a nanoparticle array.

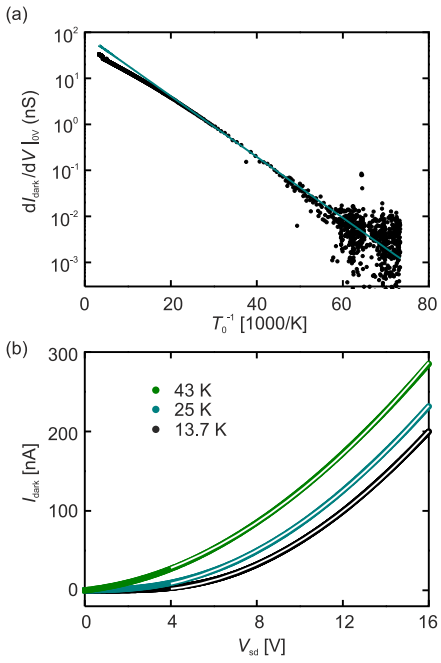

Figure 2. (a) Differential conductance at zero applied bias $dI/dV|_{0V}$ on a logarithmic scale as a function of the inverse temperature (black dots). The blue line represents a linear fit to the data. (b) Current−voltage characteristic of a nanoparticle array measured at $T = 13.7$ K (black symbols), $T = 25$ K (blue symbols), and $T = 43$ K (green symbols). The white lines represent fits to the data using eq 1, with $\xi = 1.943 \pm 0.003$ and $V_t = 2.79 \pm 0.01$, 1.35 ± 0.02, and -1.23 ± 0.02 V at $T_0 = 13.7$, 25, and 43 K, respectively.

the potential landscape and, by this, to a strong field enhancement in the rest of the array.

Our interpretation is substantiated by the results of a two-beam photoconductance investigation. We use two individually controllable laser beams for the local optical excitation of the array, as is sketched in Figure 1a. In such a scheme, we can influence the electric field at the position of beam I by the use of beam II. In the case of the two-beam excitation, we observe a negative differential photoconductance across the nanoparticle array. The occurrence of a negative differential photoconductance is fully consistent with our model of an inhomogeneous temperature profile and the redistribution of the potential landscape in the nanoparticle array. Our results show that gold nanoparticle arrays in the Coulomb blockade regime are very sensitive to a local lift of the Coulomb blockade. Therefore, we can obtain local control of the electric transport in a nanoparticle array by optical means. This can be interesting for applications as optical sensors or for local temperature measurements.

RESULTS AND DISCUSSION

We examine two-dimensional arrays consisting of hexagonally ordered gold particles with a diameter of ~10 nm.[16] Octanethiols coating the nanoparticles serve as spacer molecules. This results in an interparticle spacing of ~2−3 nm. In Figure 1b, we present a scanning electron microscope (SEM) image of such a nanoparticle array. Twenty micrometer wide strips of nanoparticle arrays are patterned on a SiO_2 substrate by a microcontact printing technique.[17] The strips are contacted by macroscopic gold electrodes with a distance of 8 μm. This scheme results in electrically contacted stretches of a nanoparticle array with a size of $8 \times 20\ \mu m^2$.

Dark Conductance of Nanoparticle Arrays. For measurements of the electrical and optoelectronic properties of the nanoparticle arrays, they are introduced in a helium flow cryostat with an optical window. The mechanism of charge transport in an assembly of metal nanoparticles strongly depends on several energy scales describing the nanoparticle assembly.[18,19] For small coupling between adjacent nanoparticles, that is, when the tunneling conductance G_{tun} is small compared to the quantum of conductance $G_0 = 2e^2/h$, with e the elementary charge and h Planck's constant, the nanoparticle assembly is in the insulating regime. In the insulating regime at low temperatures, the conductance is governed by the single electron charging energy E_c of the nanoparticles. This is the so-called Coulomb blockade regime. E_c can be overcome by thermal activation of the charge carriers. Therefore, the zero bias conductance $dI_{dark}//dV|_{0V}$ follows the Arrhenius law for a nanoparticle array in the Coulomb blockade regime. In Figure 2a, we show $dI_{dark}/dV|_{0V}$ measured with a lock-in amplifier and a modulation of $V_{mod} = 10$ mV of the bias around 0 V. $dI_{dark}/dV|_{0V}$ is shown on a logarithmic scale as a function of the inverse temperature $1/T_0$. The blue line represents a linear fit to the data. At low temperatures, the data are well described by the linear fit and thus by the

Arrhenius law. From the slope of the linear fit, we deduce $E_c = 13.1 \pm 0.1$ meV. At high temperatures (*i.e.*, for $k_B T_0 > E_c$, with k_B the Boltzmann constant), the observed temperature dependence is weaker than predicted by the Arrhenius law. This indicates that the transport is not dominated by the Coulomb blockade at this temperature.[18]

Further, the Coulomb blockade can be overcome by an applied bias. The current−voltage characteristic of a nanoparticle array is then characterized by a threshold voltage V_t, above which the current in the array increases following a power law of the applied bias V_{sd}:[20]

$$I_{dark}(V_{sd}) \propto \mathrm{sgn}(V_{sd})(|V_{sd}| - V_t)^{\xi}, \text{ for } |V_{sd}| > V_t \quad (1)$$

The exponent ξ is predicted to lie between 2 and 3 in finite two-dimensional assemblies.[21,22] In Figure 2b, we plot the current−voltage characteristic of a nanoparticle array measured at three different temperatures T_0 = 13.7, 25, and 43 K (black, blue, and green symbols, respectively). The white lines represent fits to the data for $V_{sd} > 4$ V using eq 1. Best fit is achieved with $\xi = 1.943 \pm 0.003$ at all temperatures. This value is very robust with regard to changes in the fitted data range. For the threshold voltage, we observe a linear decrease of V_t with increasing temperature. At $T_0 = 43$ K, we observe a negative effective voltage threshold which indicates the presence of conducting paths even at zero applied bias. By an extrapolation of the obtained V_t values, we can deduce the $T = 0$ global threshold of conductance $V_t(0) = 4.74 \pm 0.08$ V. As described in detail in ref 20, $V_t(0)$ is linked to the Coulomb charging energy E_c by

$$eV_t(0) = 2\alpha N E_c \quad (2)$$

where N is the number of nanoparticles between the contacts and $\alpha = 0.226$ is a constant defined by the array topology. We determine $N = 713 \pm 100$ from SEM images of the nanoparticle array. Thus, we calculate $E_c = 14.7 \pm 2.2$ meV, which agrees with the value obtained from the Arrhenius fit within the experimental error.

Spatially Resolved Photocurrent. In Figure 3a, we show an SEM image of a contacted strip of nanoparticle array. To perform optoelectronic measurements on the nanoparticle arrays, we focus the light of a mode-locked titanium sapphire laser through the objective of a microscope on our sample surface. Laser light is available with photon energies of 1.24 eV < E_{photon} < 3.44 eV (see Methods for details). To obtain a two-dimensional image of our sample, we scan the laser beam in *x*- and *y*-direction with respect to our sample. First, we measure the intensity of the reflected light. The contacted strip of the nanoparticle array can be clearly recognized in the reflection map shown in Figure 3b. Simultaneously, we measure the optically induced current I_{photo}. The two-dimensional map of I_{photo} shown in Figure 3c reveals that a photocurrent is induced when irradiating the area covered with nanoparticles. In contrast, there is no I_{photo} when irradiating either the gold electrodes or the empty area next to the nanoparticle array.

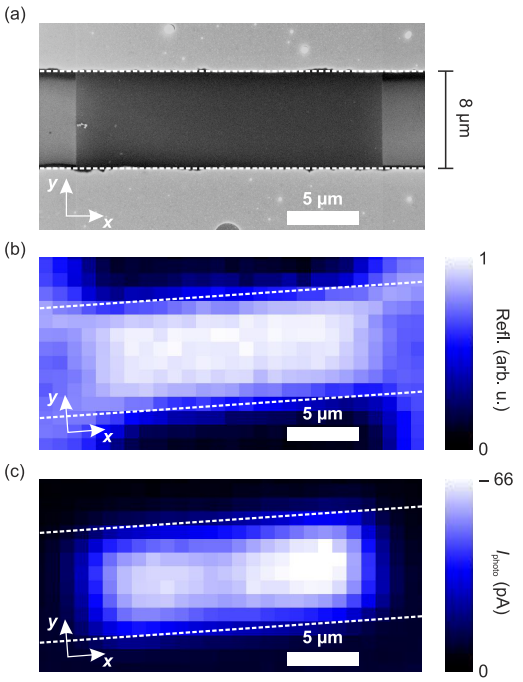

Figure 3. (a) SEM image of a 20 μm wide strip of nanoparticle array electrically contacted by gold electrodes. (b) Two-dimensional map of the reflection of a focused laser beam from the sample surface. (c) Optically induced current I_{photo} measured concurrently with the reflection in (b). (b,c) E_{photon} = 2.07 eV, I_{opt} = 0.7 kW/cm^2, V_{sd} = −3 V, f_{chop} = 1764 Hz, and T_0 = 16.9 K (see Methods for acronyms).

Redistribution of the Potential Landscape. The $I_{photo}-V_{sd}$ characteristic of a nanoparticle array at T_0 = 13.7 K is shown in black in Figure 4a. The measurements are performed at E_{photon} = 2.07 eV. Qualitatively similar results are obtained for all experimentally accessible E_{photon}. We observe a small increase of I_{photo} for $|V_{sd}| <$ 2 V (region I in Figure 4a), a strong increase of I_{photo} at an intermediate bias (region II), and a reduced increase of I_{photo} for $|V_{sd}| > 10$ V (region III). In blue, we show the equivalent measurement at T_0 = 25 K. At this elevated T_0, the region of vanishing I_{photo} at small V_{sd} disappears. We further point out that we measure a distinctively smaller photocurrent at a higher temperature.

In a simplified model, this behavior can be explained with a lifted Coulomb blockade due to a local temperature increase of the nanoparticle array. Figure 4b depicts a sketch of a nanoparticle array irradiated by a laser beam. The sample is at a temperature T_0. At the excitation position, the temperature is locally increased to T_1. On the basis of the data in Figure 2b, an increased temperature leads to an increased conductance of the nanoparticle array. Generally, without irradiation, the potential U can be assumed to drop linearly between the two contacts because of the large number of nanoparticles between

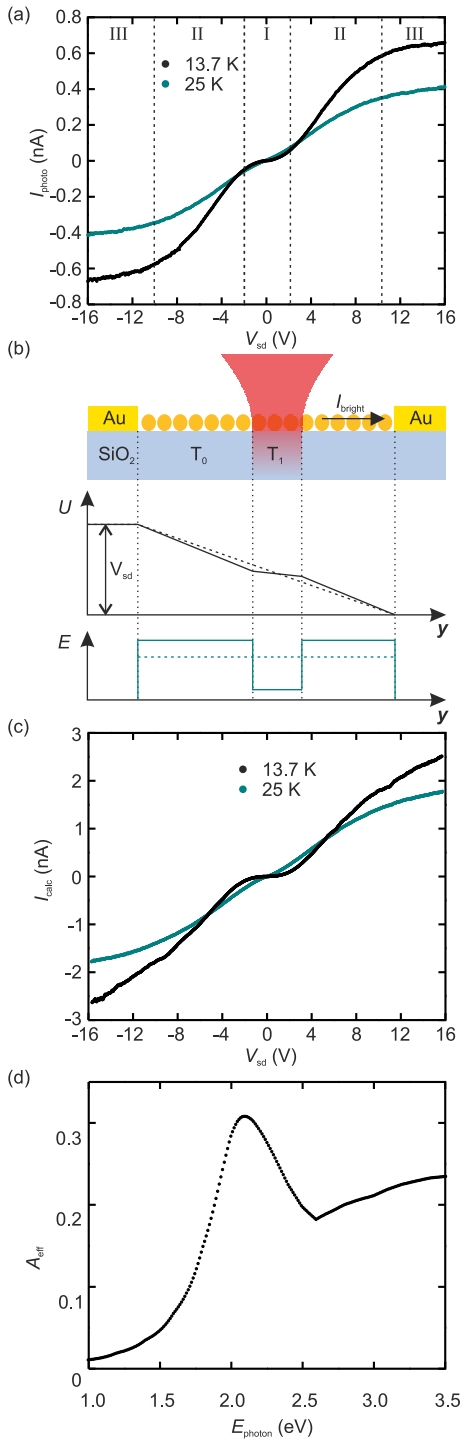

Figure 4. (a) I_{photo} as a function of V_{sd} measured at $T = 13.7$ K (black) and $T = 25$ K (blue) ($E_{photon} = 2.07$ eV, $I_{opt} = 0.7$ kW/cm^2, and $f_{chop} = 1605$ Hz). (b) Sketch of a nanoparticle array at bath temperature T_0 on a SiO_2 substrate contacted by gold electrodes and irradiated by a focused laser beam increasing the local temperature to T_1. Second and third panel represent the potential U and the electric field E as a function of position in the irradiated (solid line) and the non-irradiated (dashed line) array. (c) Calculated photocurrent I_{calc} as a function of V_{sd} for $T_0 = 13.7$ K, $T_1 = 16.2$ K (black) and $T_0 = 25$ K, $T_1 = 26.6$ K (blue). (d) Calculated absorption A_{eff} of a nanoparticle array as a function of the photon energy E_{photon}.

the two contacts (indicated as a dashed line in the second panel of Figure 4b). Under irradiation, the potential drop in the irradiated area is reduced due to the locally increased conductance. Consequently, the potential drop in the non-irradiated area must increase such that the overall potential drop equals the applied bias V_{sd} (solid line in the second panel of Figure 4b). The electric field is assumed to be constant along the non-irradiated array (dashed line in the third panel of Figure 4b). Under irradiation, the electric field is reduced in the irradiated sample part, while it is increased in the non-irradiated sample part (solid line).

According to this scheme, we can calculate I_{photo} from the measured temperature dependence of the current–voltage characteristic of the non-irradiated array shown in Figure 2b. The dark conductance measurements are performed for T_0 = 13.7, 19, 25, and 43 K. The current–voltage characteristics at other bath temperatures are obtained by linear interpolation of the data in Figure 2b. We motivate this method by the small temperature increase in the experiment. The current in the non-irradiated sample part is given by $I_0 = I_{dark}(T_0,E)$, with the electric field E in first approximation given by the applied bias divided by the length l of the nanoparticle array, $E = V_{sd}/l$. Accordingly, the current in the irradiated sample part is given by $I_1 = I_{dark}(T_1,E)$. In a recursive calculation, the electric fields in the two regions are adjusted such that they sum up to the given voltage V_{sd} and the current in the irradiated region equals the current in the non-irradiated region. As soon as I_0 and I_1 converge, the obtained value I_{bright} represents the current in a partly irradiated array. The calculated optically induced current I_{calc} is then obtained as the difference between the current in an irradiated array and the current in the non-irradiated array, $I_{calc} = I_{bright} - I_{dark}(T_0,E)$.

The temperature T_0 is equal to the temperature of the sample substrate. It is measured using a calibrated silicon diode. The temperature T_1 can be estimated from the amount of energy absorbed by the nanoparticle array.[23] In thermal equilibrium, the absorbed power must be equal to the power that is tranported away from the nanopartricle array through the underlying substrate. As discussed in detail in ref 13, the temperature of the array can be assumed to be locally increased by

$$\Delta T = \frac{I_{opt} A_{eff} d_{SiO_2}}{\lambda_{SiO_2}} \qquad (3)$$

with I_{opt} the irradiation intensity, A_{eff} the absorption of the array (for a discussion of A_{eff} see below), and d_{SiO_2} and λ_{SiO_2} the thickness and thermal conductivity of the SiO_2 substrate, respectively. For the experimental conditions of the measurements shown in Figure 4a (I_{opt} = 0.7 kW/cm^2, A_{eff} = 0.31, d_{SiO_2} =150 nm), we calculate $\Delta T_{13.7K} = 2.5$ K using $\lambda_{SiO_2} = 0.13$ W/(m·K) at $T_0 = 13.7$ K and $\Delta T_{25K} = 1.6$ K using $\lambda_{SiO_2} = 0.20$ W/(m·K) at $T_0 = 25$ K.[24]

I_{calc} for $T_0 = 13.7$ K and $T_1 = T_0 + \Delta T_{13.7K} = 16.2$ K is plotted as black symbols in Figure 4c. The calculated

curve agrees qualitatively very well with the measured curve in Figure 4a. The blue symbols in Figure 4c represent I_{calc} calculated with $T_0 = 25$ K and $T_1 = T_0 + \Delta T_{25K} = 26.6$ K. We can reproduce the smaller photocurrent at the elevated bath temperature as well as the nonvanishing photocurrent at small applied bias.

Thanks to the successful application of the model, we can identify the physical origin of the three different regimes in the photocurrent measurement. At small bias $|V_{sd}| < 2$ V (region I) and at $T_0 = 13.7$ K, the nonirradiated area of the nanoparticle array is still in the Coulomb blockade regime despite the increase of the electric field due to irradiation. Thus, the overall current is very small even under irradiation. At $T_0 = 25$ K, a small optically induced increase of the electric field can partially lift the Coulomb blockade in the nanoparticle array. Thus, the photocurrent increases more quickly at an elevated bath temperature. When the static electric field provided by the bias voltage is large enough to overcome the Coulomb blockade even at $T_0 = 13.7$ K, we observe a strong increase of the photocurrent. This corresponds to region II in the measurements. In region III, the photocurrent increases less with increasing bias. This is due to the much weaker temperature dependence of the dark conductance at high bias. The smaller photocurrent in region III at $T_0 = 25$ K compared to $T_0 = 13.7$ K is due to the reduced temperature increase at the higher bath temperature.

To clarify the underlying heating mechanism, we investigate the photoconductance at a range of photon energies E_{photon} of the exciting light. Generally, the absorption spectrum of gold nanoparticle arrays is dominated by the excitation of strongly interacting surface plasmons in the gold particles.[25,26] The Maxwell–Garnett effective medium theory allows one to calculate the absorption A_{eff} of a nanoparticle array from the bulk dielectric properties of gold and the organic matrix.[27−29] In Figure 4d, we show the absorption as a function of E_{photon} of a nanoparticle array with octane thiol molecules as organic matrix. The calculation was performed as described in detail in ref 13. The broad maximum of absorption centered at ~2 eV is due to the excitation of surface plasmons in the nanoparticles.[30] The increase of absorption for photon energies higher than ~2.6 eV is caused by interband excitations in the gold particles.[31] In our experiments, we optically excite our samples with photons which are resonant with the surface plasmon excitation or the interband transition in gold. Additionally, we optically excite the arrays in the infrared spectral range resonant with none of the mentioned transitions. We observe the same qualitative behavior independent of E_{photon}. Due to the dispersive nature of the mentioned transitions, the absorbed energy is quickly transformed in an increase of the bath temperature of the nanoparticle array.[23] Thus, we interpret our findings to be caused by a temperature increase of the nanoparticle array.

Further, we can change the composition of the organic matrix of the arrays by the introduction of oligo(phenylene vinylene) (OPV).[17,32] By this, we can excite a single electron transition in the organic matrix with $E_{photon} \approx 3.3$ eV.[33] This results in a resonant molecular photoconductance which appears in addition to a bolometrically induced conductance.[34] The results shown above and in the following are obtained with samples with OPV in the organic matrix. However, the results described here are found to be independent of the composition of the organic matrix. This corroborates the interpretation that an induced temperature increase is responsible for the observed photoconductance rather than an electronic excitation in the nanoparticles or the organic matrix.

Negative Differential Photoconductance. A major assumption of the discussed model is that the local optical excitation gives rise to an increase of the electric field in the rest of the current path. To test this assumption, we introduce a method using two laser beams (beam I and beam II) to optically excite the nanoparticle array. The two beams can be independently positioned on the sample. By this, we can use beam I to manipulate the electric field at the position of beam II. The two beams are chopped at two different frequencies. We measure the current component I_{photo}^{2beam} at the sum of the two frequencies. By this, we are sensitive to the modulation of the photocurrent of one beam by the other beam. In other words, we measure how much the optically induced current differs from being the sum of the optically induced currents of beam I and beam II (see Supporting Information). In Figure 5a, we show a sketch of the described measurement setup. The dashed area represents the nanoparticle array which is contacted by source and drain electrode (depicted in gray). Beam II can be moved relative to beam I in the *x*- and the *y*-direction. In Figure 5b–f, we show $I_{photo}^{2beam}-V_{sd}$ characteristics measured with the two laser beams with $E_{photon,1} = 3.26$ eV and $E_{photon,2} = 2.07$ eV, respectively. We want to note that we observe qualitatively similar results for any combination of colors of the two beams. Also, the results are independent of the composition of the organic matrix of the nanoparticle array (data not shown).

When the two laser beams excite exactly the same spot of the array, I_{photo}^{2beam} depends on V_{sd} as shown in Figure 5b. In the inset of Figure 5b, we show the position of the two beams (blue circle for $E_{photon,1} = 3.26$ eV, orange circle for $E_{photon,2} = 2.07$ eV) in a reflection map of the sample. We measure an $I_{photo}^{2beam}-V_{sd}$ characteristic which is qualitatively similar to the one observed with only one laser beam: I_{photo}^{2beam} increases weakly at a small bias, followed by a strong increase in an intermediate bias regime and a reduced increase of I_{photo}^{2beam} for $|V_{sd}| > 10$ V. However, please note the opposite sign of I_{photo}^{2beam} compared to the measurement with only one beam. We refer to this effect as the negative contribution to the photocurrent. The negative

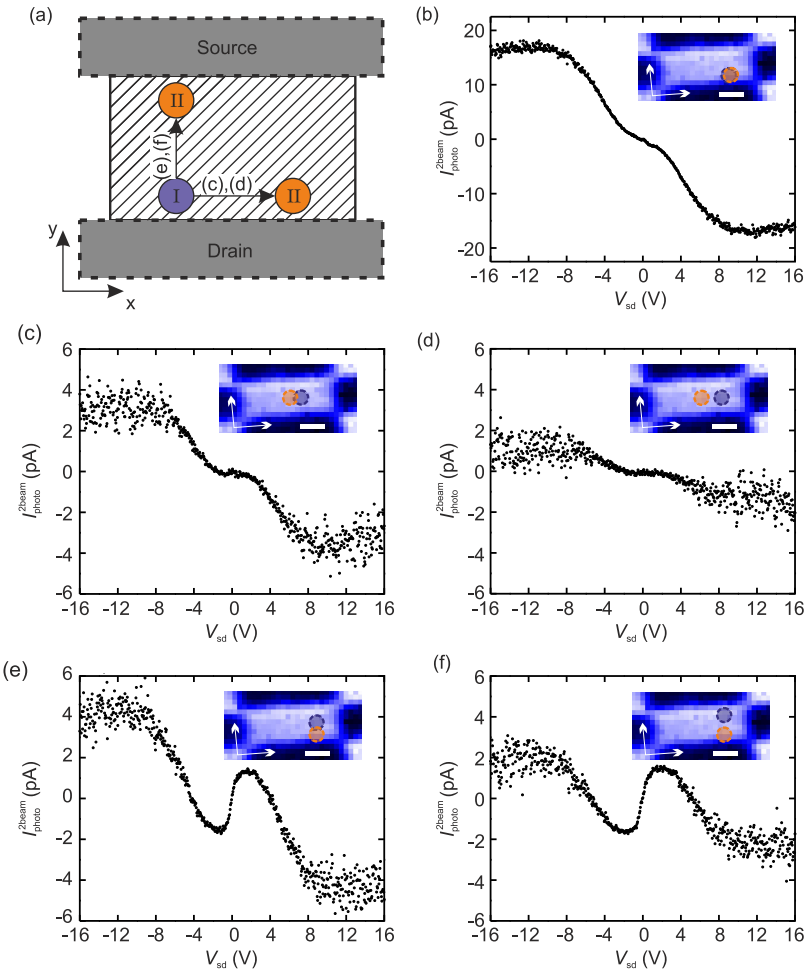

Figure 5. (a) Sketch of the two-beam measurement setup. Beam II (orange circle) can be moved relative to beam I (blue circle) in *x*- and in *y*-direction. (b−f) Photocurrent induced by two laser beams as a function of V_{sd} for the two beams (b) at the same position, (c) with an offset of 2 μm in *x*-direction, (d) an offset of 4 μm in *x*-direction, (e) an offset of 2 μm in *y*-direction, and (f) an offset of 4 μm in *y*-direction. The inset shows a two-dimensional reflection map with the position of beam I (blue circle) and beam II (orange circle) marked ($E_{photon,1}$ = 3.26 eV, $I_{opt,1}$ = 0.35 kW/cm^2, $E_{photon,2}$ = 2.07 eV, $I_{opt,2}$ = 0.71 kW/cm^2, f_{chop} = 3540 Hz, T_0 = 13.7 K, scale bar = 5 μm).

contribution requires an overlap of the two laser beams. This is illustrated by the measurements shown in Figure 5c,d. For the results shown in Figure 5c, the two beams are moved by approximately 2 μm in *x*-direction relative to each other. The reduced overlap of the two beams leads to a reduction of I^{2beam}_{photo} at V_{sd} = 16 V from ∼17 to ∼3 pA. For the measurement depicted in Figure 5d, the two beams are at a distance of ∼4 μm. This leads to an almost complete suppression of the negative contribution to I^{2beam}_{photo}.

The negative contribution is also suppressed when the two laser beams are displaced in *y*-direction relative to each other. In Figure 5e, the two beams have a distance of ∼2 μm in *y*-direction, which leads to a reduction of I^{2beam}_{photo} at V_{sd} = 16 V to ∼4 pA. At the same time, a new, positive contribution to I^{2beam}_{photo} arises for $|V_{sd}| < 5$ V. It is of opposite sign compared to the negative contribution discussed so far. This positive photocurrent contribution does not require an overlap of the two laser beams. In contrary, we find that it only arises when the two beams are at least partially not overlapping. When the two beams are shifted in *y*-direction even more (Figure 5f), the positive contribution is sustained while the negative photocurrent contribution is nearly completely suppressed.

As we discuss below, the observation of a positive as well as a negative contribution to the photocurrent corroborates the interpretation of the photoconductance mechanism as sketched above. In Figure 6a, we show a schematic representation of the situation when the two laser beams are shifted in *y*-direction relative to each other such that they still have a significant overlap. We assume that the non-irradiated sample is at a temperature T_0. At the positions where only one beam is incident on the sample, the temperature is increased to a value $T_1 > T_0$. To simplify the reasoning as well as the calculations, the temperature induced by the two individual beams is assumed to be equal. Assuming different temperatures, however, does not change the underlying arguments. At the position where the two

beams overlap, the temperature is increased to $T_2 > T_1$. Due to the higher dark conductance at a higher temperature, the potential drop and the local electric field are reduced at positions with an increased temperature, as is sketched in the second and the third panel in Figure 6a.

Again, we obtain the current in the different regions of the nanoparticle array from the linear interpolation of the temperature dependence of the dark current. In the recursive calculation, the electric fields in the three temperature regions are adjusted such that the current flow is the same in all regions. The current value I^{2beam}_{bright} obtained upon convergence is the entire current in a nanoparticle array illuminated by the two laser beams. The current which is experimentally detected at the sum frequency is then given by the following expression (see Supporting Information):

$$I^{2beam}_{calc} = I^{2beam}_{bright} - I_{dark} - I_{photo,1} - I_{photo,2} \quad (4)$$

with I^{2beam}_{bright} the current obtained in the recursive calculation, I_{dark} the dark current at $T = T_0$, and $I_{photo,1/2}$ the photocurrent induced when only beam I/II is present.

In Figure 6b, we show I^{2beam}_{calc} for two 3 μm wide laser beams with an assumed overlap of 95%. The calculated temperatures are $T_0 = 13.7$ K, $T_1 = T_0 + \Delta T_{13.7K} = 16.2$ K, and $T_2 = T_0 + 2\Delta T_{13.7K} - 0.1$ K $= 18.6$ K. In order to reproduce the overall negative slope of the $I^{2beam}_{photo} - V_{sd}$ characteristic, we have to assume a temperature increase in the region irradiated by both beams which is slightly less than two times $\Delta T_{13.7K}$. Due to this, the effect of the second beam is reduced and we measure an apparent negative differential photoconductance. The reduced temperature increase reflects the increase of the thermal conductivity λ_{SiO_2} of the substrate at higher temperatures. Again, the small I^{2beam}_{photo} for $V_{sd} < 2$ V is caused by the Coulomb blockade, and the reduced increase for $V_{sd} > 10$ V is due to a weak temperature dependence of the current–voltage characteristic at a large applied bias.

Reducing the overlap of the two laser beams in the calculation reproduces the positive contribution to the photocurrent. In Figure 6c, we show I^{2beam}_{calc} for two 3 μm wide laser beams with only 35% overlap. The positive contribution to the photocurrent, that is, the fact that the current induced by two beams is higher than the sum of the currents induced by the two individual beams, is due to the strong increase of the electric field in the non-irradiated region of the nanoparticle array. By this, under double irradiation the Coulomb blockade is overcome at a smaller bias than under irradiation by only one beam. This leads to the strongly enhanced optically induced current.

CONCLUSION

In conclusion, we investigate the photoconductance of gold nanoparticle arrays in the Coulomb blockade regime. We observe a strong enhancement of the conductance due to optical excitation of the arrays. We propose a model based on a local temperature increase induced by the laser beam. The inhomogeneous temperature profile leads to a redistribution of the potential landscape in the array. Applying this model, we can calculate the observed photocurrent from the dark current–voltage characteristic of the array. The same model can be applied to calculate the photocurrent induced by two individually positioned laser beams. When the two laser beams are overlapping, the induced temperature increase is less than the sum of the temperature increases induced by each of the individual laser beams. Due to this, we observe a reduced induced photocurrent and thus a negative differential photoconductance. When the

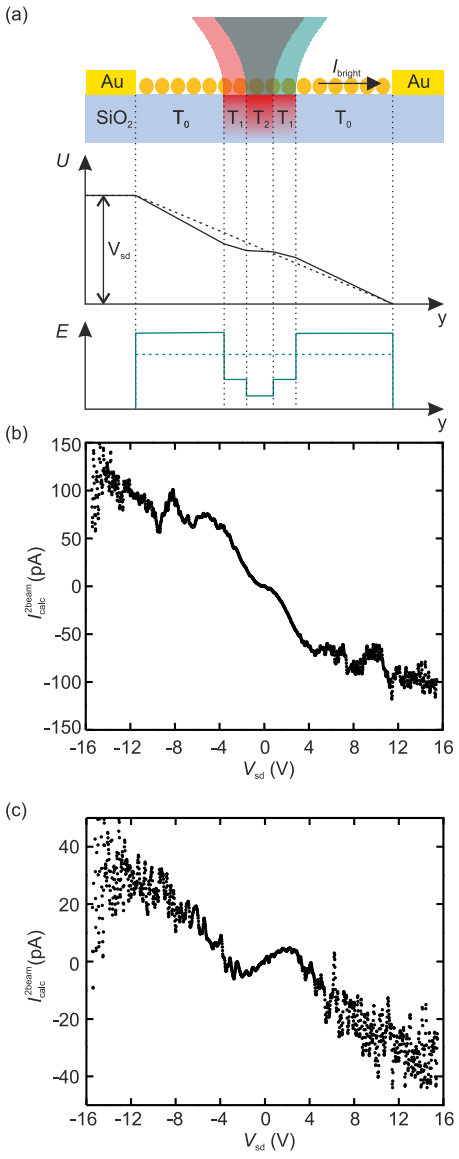

Figure 6. (a) Scheme of a nanoparticle array at bath temperature T_0 irradiated by two laser beams. Second and third panel show schematically the potential U and the electric field E as a function of position. (b) I_{calc} calculated under irradiation with two 3 μm wide beams as a function of V_{sd} for $T_0 = 13.7$ K, $T_1 = 16.2$ K, $T_2 = 18.6$ K and an overlap of the two beams of (b) 95% and (c) 35% (see text for further details).

two beams are displaced relative to each other in direction of the current flow, the redistribution of the potential landscape can lead to an enhancement of the electric field in the non-irradiated array. Due to the large electric field, the Coulomb blockade can be lifted in the nanoparticle array. By this, the photocurrent induced by the two laser beams can be much larger than the sum of the photocurrents induced by each of the beams. This leads to the observation of a positive differential photoconductance.

Our results show that the current flow in nanoparticle arrays in the Coulomb blockade regime can be spatially controlled using local optical excitations. This opens the possibility of spatially resolved temperature or optical sensing using two-dimensional nanoparticle assemblies.

METHODS

Array Preparation. The gold nanoparticles were prepared by reduction of Au(III) as described in ref 35. Twenty milliliters of a heated reducing solution (0.2% (by weight) citric acid trisodium salt, 0.004% (by weight) tannic acid) was added to 80 mL of a boiling solution of 1% (by weight) $HAuCl_4$; the mixture was boiled under stirring for 10 min, then cooled to room temperature. This resulted in Cl^--stabilized gold particles with a mean diameter of ~9.5 nm, as was confirmed by X-ray scattering.[16]

Formation of the nanoparticle array followed a protocol proposed by Huang *et al.*[36] Ten milliliters of the Au nanoparticle solution was centrifuged for 60 min at 14 krpm and the supernatant water was removed. The sedimented nanoparticles were dissolved in 10 mL of ethanol, and 4 mL of a 2.4% (by volume) solution of freshly distilled octanethiol in ethanol was added. The octanethiols were bound to the gold nanoparticles overnight and the alkane-coated particles precipitated. The supernatant ethanol was removed the next day, and the sediment was washed in fresh ethanol. After a new precipitation, the ethanol was removed and the nanoparticles were dissolved in 3.5 mL of chloroform.

For the self-assembly of the nanoparticle array, 350 μL of the nanoparticles dissolved in chloroform was casted on a water surface confined in a Teflon ring. The array was transferred from the water surface to a Si chip with 150 nm thermally grown SiO_2 using a polydimethylsiloxane (PDMS) stamp. By this procedure, we produced two-dimensional, hexagonally ordered nanoparticle arrays with a lattice spacing of ~12 nm and an interparticle distance of ~2 nm, as shown in the scanning electron microscope (SEM) image in Figure 1b.

Gold electrodes were patterned on the arrays using a shadow mask evaporation technique. The electrodes were evaporated at a distance of 8 μm on a 20 μm wide strip of nanoparticle array, leaving an 8 $\times$ 20 μm^2 sized electrically contacted nanoparticle array.[13]

Molecular Exchange. The incorporation of OPV into the nanoparticle array follows the method described in ref 17. The OPV-thiols with an acetylene protection group were dissolved in 2 mL of tetrahydrafuran (THF) to yield a 1 mM solution. The chip with the nanoparticle array was added to the vial, and the vial was purged with Ar. Ten microliters of a 10% aqueous solution of ammonium hydroxide (NH_4OH) was added to remove the protection from the thiol groups of the OPV. The solution was kept under Ar atmosphere for 24 h. When the chip was removed, it was first washed in THF to remove unbound OPV, then it was washed in ethanol, and after that, it was blown dry with N_2. This results in the interconnection of the Au nanoparticles by the OPV molecules.[17] The introduction of the OPV increased the conductance of the arrays by approximately 1 order of magnitude (data not shown).

Photoconductance Measurements. Photoconductance measurements were performed under high vacuum conditions (~10^{-6} mbar) in a liquid helium flow cryostat at temperature T_0. For optical excitation, we used a mode-locked titanium:sapphire laser with optical pulses of ~160 fs duration and a repetition rate of 76 MHz. To cover the UV spectral range, the frequency of the light was doubled using a BBO crystal. The visible spectrum was covered by supercontinuum generation in a nonlinear optical fiber and subsequent wavelength selection using diffraction filters. By means of a chopper wheel, the optical excitation was modulated with a frequency f_{chop}. A DC bias V_{sd} was applied to the electrically contacted nanoparticle array with a Yokogawa voltage source, and the resulting current was amplified in an Ithaco Model 1211 current–voltage converter. The optically induced current I_{photo} was determined as the current component at f_{chop} measured with an EG&G 7265 lock-in amplifier.

Conflict of Interest: The authors declare no competing financial interest.

Acknowledgment. We thank C. Schönenberger for support. This work was supported by the European Commission under the FP7-NMP project Hysens (263091). We further acknowledge the "Nanosystems Initiative Munich" (NIM) and the Swiss Nanoscience Institute (SNI) for funding.

Supporting Information Available: Discussion of the dual-beam measurement scheme. This material is available free of charge *via* the Internet at http://pubs.acs.org.

REFERENCES AND NOTES

1. van Staveren, M. P. J.; Brom, H. B.; de Jongh, L. J. Metal-Cluster Compounds and Universal Features of the Hopping Conductivity of Solids. *Phys. Rep.* **1991**, *208*, 1–96.
2. Zabet-Khosousi, A.; Dhirani, A. A. Charge Transport in Nanoparticle Assemblies. *Chem. Rev.* **2008**, *108*, 4072–4124.
3. Geerligs, L. J.; Anderegg, V. F.; van der Jeugd, C. A.; Romijn, J.; Mooij, J. E. Influence of Dissipation on the Coulomb Blockade in Small Tunnel Junctions. *Europhys. Lett.* **1989**, *10*, 79.
4. Orr, B. G.; Jaeger, H. M.; Goldman, A. M.; Kuper, C. G. Global Phase Coherence in Two-Dimensional Granular Superconductors. *Phys. Rev. Lett.* **1986**, *56*, 378–381.
5. Markovich, G.; Collier, C. P.; Heath, J. R. Reversible Metal-Insulator Transition in Ordered Metal Nanocrystal Monolayers Observed by Impedance Spectroscopy. *Phys. Rev. Lett.* **1998**, *80*, 3807–3810.
6. Beecher, P.; Quinn, A. J.; Shevchenko, E. V.; Weller, H.; Redmond, G. Insulator-to-Metal Transition in Nanocrystal Assemblies Driven by *In Situ* Mild Thermal Annealing. *Nano Lett.* **2004**, *4*, 1289–1293.
7. Zabet-Khosousi, A.; Trudeau, P.-E.; Suganuma, Y.; Dhirani, A.-A.; Statt, B. Metal to Insulator Transition in Films of Molecularly Linked Gold Nanoparticles. *Phys. Rev. Lett.* **2006**, *96*, 156403.
8. Abeles, B.; Sheng, P.; Coutts, M. D.; Arie, Y. Structural and Electrical Properties of Granular Metal Films. *Adv. Phys.* **1975**, *24*, 407–461.
9. Quinn, A. J.; Beecher, P.; Iacopino, D.; Floyd, L.; De Marzi, G.; Shevchenko, E. V.; Weller, H.; Redmond, G. Manipulating the Charging Energy of Nanocrystal Arrays. *Small* **2005**, *1*, 613–618.
10. Wang, G. R.; Wang, L.; Rendeng, Q.; Wang, J.; Luo, J.; Zhong, C. J. Correlation between Nanostructural Parameters and Conductivity Properties for Molecularly-Mediated Thin Film Assemblies of Gold Nanoparticles. *J. Mater. Chem.* **2006**, *17*, 457–462.
11. Kane, J.; Ong, J.; Saraf, R. F. Chemistry, Physics, and Engineering of Electrically Percolating Arrays of Nanoparticles: A Mini Review. *J. Mater. Chem.* **2011**, *21*, 16846–16858.

12. Talapin, D. V.; Lee, J. S.; Kovalenko, M. V.; Shevchenko, E. V. Prospects of Colloidal Nanocrystals for Electronic and Optoelectronic Applications. *Chem. Rev.* **2010**, *110*, 389–458.
13. Mangold, M. A.; Weiss, C.; Calame, M.; Holleitner, A. W. Surface Plasmon Enhanced Photoconductance of Gold Nanoparticle Arrays with Incorporated Alkane Linkers. *Appl. Phys. Lett.* **2009**, *94*, 161104.
14. Banerjee, P.; Conklin, D.; Nanayakkara, S.; Park, T. H.; Therien, M. J.; Bonnell, D. A. Plasmon-Induced Electrical Conduction in Molecular Devices. *ACS Nano* **2010**, *4*, 1019–1025.
15. Nakanishi, H.; Bishop, K. J. M.; Kowalczyk, B.; Nitzan, A.; Weiss, E. A.; Tretiakov, K. V.; Apodaca, M. M.; Klajn, R.; Stoddart, J. F.; Grzybowski, B. A. Photoconductance and Inverse Photoconductance in Films of Functionalized Metal Nanoparticles. *Nature* **2009**, *460*, 371–375.
16. Mangold, M. A.; Niedermeier, M. A.; Rawolle, M.; Dirks, B.; Perlich, J.; Roth, S. V.; Holleitner, A. W.; Müller-Buschbaum, P. Correlation between Structure and Optoelectronic Properties in a Two-Dimensional Nanoparticle Assembly. *Phys. Status Solidi RRL* **2011**, *5*, 16–18.
17. Liao, J.; Bernard, L.; Langer, M.; Schönenberger, C.; Calame, M. Reversible Formation of Molecular Junctions in 2D Nanoparticle Arrays. *Adv. Mater.* **2006**, *18*, 2444–2447.
18. Beloborodov, I. S.; Lopatin, A. V.; Vinokur, V. M.; Efetov, K. B. Granular Electronic Systems. *Rev. Mod. Phys.* **2007**, *79*, 469–518.
19. Efetov, K. B.; Tschersich, A. Coulomb Effects in Granular Materials at Not Very Low Temperatures. *Phys. Rev. B* **2003**, *67*, 174205.
20. Elteto, K.; Antonyan, E. G.; Nguyen, T. T.; Jaeger, H. M. Model for the Onset of Transport in Systems with Distributed Thresholds for Conduction. *Phys. Rev. B* **2005**, *71*, 064206.
21. Parthasarathy, R.; Lin, X.-M.; Elteto, K.; Rosenbaum, T. F.; Jaeger, H. M. Percolating through Networks of Random Thresholds: Finite Temperature Electron Tunneling in Metal Nanocrystal Arrays. *Phys. Rev. Lett.* **2004**, *92*, 076801.
22. Parthasarathy, R.; Lin, X.-M.; Jaeger, H. M. Electronic Transport in Metal Nanocrystal Arrays: The Effect of Structural Disorder on Scaling Behavior. *Phys. Rev. Lett.* **2001**, *87*, 186807.
23. Govorov, A. O.; Zhang, W.; Skeini, T.; Richardson, H.; Lee, J.; Kotov, N. A. Gold Nanoparticle Ensembles as Heaters and Actuators: Melting and Collective Plasmon Resonances. *Nanoscale Res. Lett.* **2006**, *1*, 84–90.
24. Zeller, R. C.; Pohl, R. O. Thermal Conductivity and Specific Heat of Noncrystalline Solids. *Phys. Rev. B* **1971**, *4*, 2029–2041.
25. Ghosh, S. K.; Pal, T. Interparticle Coupling Effect on the Surface Plasmon Resonance of Gold Nanoparticles: From Theory to Applications. *Chem. Rev.* **2007**, *107*, 4797–4862.
26. Thomas, K. G.; Kamat, P. V. Chromophore-Functionalized Gold Nanoparticles. *Acc. Chem. Res.* **2003**, *36*, 888–898.
27. Garnett, J. C. Colours in Metal Glasses and in Metallic Films. *Philos. Trans. R. Soc., A* **1904**, *203*, 385.
28. Genzel, L.; Martin, T. P. Infrared Absorption by Surface Phonons and Surface Plasmons in Small Crystals. *Surf. Sci.* **1973**, *34*, 33–49.
29. Ung, T.; Liz-Marzán, L. M.; Mulvaney, P. Gold Nanoparticle Thin Films. *Colloids Surf., A* **2002**, *202*, 119–126.
30. Bernard, L.; Kamdzhilov, Y.; Calame, M.; van der Molen, S. J.; Liao, J.; Schönenberger, C. Spectroscopy of Molecular Junction Networks Obtained by Place Exchange in 2D Nanoparticle Arrays. *J. Phys. Chem. C* **2007**, *111*, 18445–18450.
31. Christensen, N. E.; Seraphin, B. O. Relativistic Band Calculation and the Optical Properties of Gold. *Phys. Rev. B* **1971**, *4*, 3321–3344.
32. Liao, J.; Mangold, M. A.; Grunder, S.; Mayor, M.; Schönenberger, C.; Calame, M. Interlinking Au Nanoparticles in 2D Arrays *via* Conjugated Dithiolated Molecules. *New J. Phys.* **2008**, *10*, 065019.
33. López-Martínez, E. I.; Rodríguez-Valdez, L. M.; Flores-Holguín, N.; Márquez-Lucero, A.; Glossman-Mitnik, D. Theoretical Study of Electronic Properties of Organic Photovoltaic Materials. *J. Comput. Chem.* **2009**, *30*, 1027–1037.
34. Mangold, M. A.; Calame, M.; Mayor, M.; Holleitner, A. W. Resonant Photoconductance of Molecular Junctions Formed in Gold Nanoparticle Arrays. *J. Am. Chem. Soc.* **2011**, *133*, 12185–12191.
35. Slot, J. W.; Geuze, H. J. A New Method for Preparing Gold Probes for Multiplelabeling Cytochemisty. *Eur. J. Cell Biol.* **1985**, *38*, 87–93.
36. Huang, S.; Tsutsui, G.; Sakaue, H.; Shingubara, S.; Takahagi, T. Formation of a Large-Scale Langmuir–Blodgett Monolayer of Alkanethiol-Encapsulated Gold Particles. *J. Vac. Sci. Technol., B* **2001**, *19*, 115–120.